A unique air-assisted DMSO-oxidation pathway for the highly efficient synthesis of

2,5-diformylfuran from 5-hydroxymethylfurfural/fructose

Yujia Pang,[†a] Ning Chen,[†a] Zhizhou Zhao,[a] Lei Zhang,[b] J.O.P. Broekman,[c] Junnan Wei,*[a]

Xiujuan Li,[a] Lu Lin [d] and He Huang *[a]

[a] College of Food Science and Pharmaceutical Engineering, Nanjing Normal University,

Nanjing 210009, China

[b] Jiangsu Key Laboratory of Marine Bioresources and Environment, Jiangsu Ocean

University, Lianyungang 222005, China.

[c] Department of Chemical Engineering (ENTEG), University of Groningen, Nijenborgh

4, 9747 AG Groningen, The Netherland.

[d] College of Energy, Xiamen University, Xiamen 361102, China.

† These two authors contributed equally.

* Corresponding author:

Junnan Wei, Email: wei_junnan @njnu.edu.cn

He Huang, Email: huangh@njnu.edu.cn

Table of Contents

Experimental

Materials

Al-MCM-41 zeolite (Si/Al=25-30) was purchased from Tianjin Yuanli Chemical Engineering Co., Ltd. 2-Methylimidazole (2-MeIM, 98%), $ZrOCl_2 \cdot 8H_2O$, $Co(NO_3)_2 \cdot 6H_2O$, fructose, 2,5-diformylfuran (DFF, 98.0%), dimethyl sulfoxide (DMSO, 99.9%), acetonitrile (MeCN, 99.9%), tetrahydrofuran (THF, 99.5%), ethanol (EtOH, 99.8%) were purchased from Macklin Biochemical Technology Co., Ltd. 5-Hydroxymethylfurfural (HMF, 99.0%) was purchased from Shanghai Aladdin Biochemical Technology Co., Ltd. All reagents were used without further treatment.

Catalyst preparation

ZrCP and ZIF-67 were synthesized via room temperature precipitation approach. In a typical preparation of ZrCP, 1.0 g $ZrOCl_2 \cdot 8H_2O$ was dissolved in 10 mL methanol. Then the prepared methanol solution of 2-methylimidazole (0.01 g/L) was added dropwise into the $ZrOCl_2$ solution under magnetic stirring at room temperature for 20 h. The resulting precipitant was recovered by centrifugation at 9000 ppm for 5 min and washed with methanol for three times. The violet sample was then dried at 80 °C under vacuum for 12 h to afford ZrCP. ZIF-67 was prepared by replacing $ZrOCl_2 \cdot 8H_2O$ with $Co(NO_3)_2 \cdot 6H_2O$ using the same method. ZrNC and CoNC were prepared through the calcination of ZrCP and ZIF-67, respectively, at 600 ºC for 4.5 h in a tube furnace under N_2 flow.

The CoZrNC-MCM catalyst were prepared through a cascade of methods including impregnation, complexation, and cation exchange. In the typical process, 1.0 g Al-MCM-41 (Si:Al=5/6) zeolite, 1.0 g $Co(NO_3)_2 \cdot 6H_2O$ and 1.0 g $ZrOCl_2 \cdot 8H_2O$ were added to 5 mL, 10 mL and 15 mL methanol, respectively, followed by mixing and magnetic stirring at room temperature for 2 h. Then the prepared methanol solution of 2-methylimidazole (0.01 g/L) was added dropwise into the above-mentioned mixed solution under magnetic stirring at room temperature for 20 h. Afterwards, the resulting solid was separated by centrifugation and washed by ultrapure water for three times, followed by being dried in a vacuum oven at 80 °C for 12 h. Finally, the

dried solid was calcined in a tube furnace under N_2 atmosphere at 600 ºC for 4.5 h to obtain the CoZrNC-MCM catalyst. For comparison purpose, CoNC-MCM, ZrNC-MCM and Co_xZr_yNC-MCM were prepared by the similar process (x and y represent the mass of $Co(NO_3)_2 \cdot 6H_2O$ and $ZrOCl_2 \cdot 8H_2O$ in the preparation process).

Catalyst characterizations

X-ray diffraction (XRD) patterns were obtained using a Bruker D8 Advance X-ray diffractometer with Cu Kα radiation from 10° to 80° at a scan speed of 8°/min. Scanning electron microscopy (SEM) (Hitachi S-4800) and transmission electron microscope (TEM) (JEM-2100) were adopted to investigate the morphology of the sample, and the element content of the sample was investigated by an Energy Dispersive Analysis of X-rays (EDAX). The specific surface area and pore size distribution of the catalyst was calculated by N_2 adsorption–desorption isotherms (Micromeritics ASAP 2020 HD88) with Brunauer-Emmett-Teller (BET) as well as Barrett-Joyner-Halenda (BJH) methods. X-ray photoelectron spectroscopy (XPS) was performed using an AXIS ULTRA spectrometer equipped with an Al Kα X-ray source. NH_3 temperature programmed desorption (NH_3-TPD) data were acquired with a Micromeritics AutoChemII-2920 instrument connected to a mass spectrometric detector. In the case of NH_3-TPD, a 100 mg sample was pre-treated in He gas at 300 °C for 60 min then cooled to 50 °C and exposed to a flow of 10% NH_3 in He at a rate of 25 ml/min for 120 min. The sample was subsequently purged with He until the baseline stabilized and then heated to 500 °C at a rate of 10 °C min^{-1}. A Bruker Tensor 27 spectrometer was used to record Fourier Transform infrared spectroscopy of pyridine (Py-FTIR). In the Py-FTIR experiment, the samples were initially pressed in a self-supporting disc (D= 13 mm), and then reduced at 60 ºC for 1 h with subsequent vacuum treatment for 3 h. Pyridine adsorption has been performed by addition of pyridine doses in the cell at room temperature till full saturation of the signal.

Catalytic reactions

HMF oxidation to DFF. The reactions were carried out in 150 mL round bottom flasks equipped with reflux condenser and magnetic stirrer. In a typical reaction, 0.2 g of

HMF, 19.8 g of DMSO and 0.08 g of catalyst were added to the flask, which was then heated to the desired reaction temperature in an oil bath and stirred to 500 rpm in the atmosphere. After the reaction, the reactor was rapidly cooled to room temperature and the catalyst was removed by filtration. The resulting liquid products were analyzed by Gas chromatography-mass spectrometry (GC-MS) using external standard method. HMF conversion (X_{HMF}) and product yield ($Y_{Product}$) were calculated by the following equations:

$$X_{HMF} \ (mol \ \%) = \left(1 - \frac{moles \ of \ detected \ HMF}{moles \ of \ starting \ HMF}\right) \times 100\%$$

$$Y_{Product} \ (mol \ \%) = \frac{moles \ of \ detected \ product}{moles \ of \ starting \ HMF} \times 100\%$$

One-step synthesis of DFF from fructose. The direct conversion of fructose to DFF was carried out in a 150 mL flask connected to a condenser to prevent solvent volatilization. In a typical process, 0.2 g of fructose, 0.08 g of catalyst and 19.8 g of DMSO were added into the flask. The flask was heated to the desired reaction temperature in an oil bath and stirred to 500 rpm in the atmosphere. After the reaction, the reactor was rapidly cooled to room temperature and the catalyst was removed by filtration. The resulting liquid products were diluted with deionized water and analyzed by high performance liquid chromatography (HPLC) using external standard method. Fructose conversion ($X_{Fructose}$), product yield ($Y_{Product}$) and selectivity ($S_{Product}$) were calculated by the following equations:

$$X_{Fructose} \ (mol \ \%) = \left(1 - \frac{moles \ of \ detected \ Fructose}{moles \ of \ starting \ Fructose}\right) \times 100\%$$

$$Y_{Product} \ (mol \ \%) = \frac{moles \ of \ detected \ product}{moles \ of \ starting \ Fructose} \times 100\%$$

Computational methods

We have employed the Vienna Ab Initio Package (VASP)[1, 2] to perform all the density functional theory (DFT) calculations within the generalized gradient approximation (GGA) using the PBE[3] formulation. We have chosen the projected augmented wave (PAW) potentials[4, 5] to describe the ionic cores and take valence electrons into account using a plane wave basis set with a kinetic energy cutoff of 400 eV. Partial occupancies of the Kohn-Sham orbitals were allowed using the Gaussian smearing method and a

width of 0.05 eV. The electronic energy was considered self-consistent when the energy change was smaller than 10^{-5} eV. A geometry optimization was considered convergent when the force change was smaller than 0.02 eV/Å. Grimme's DFT-D3 methodology[6] was used to describe the dispersion interactions.

The equilibrium lattice constant of hexagonal graphene unit cell separated by a vacuum layer in the depth of 15 Å was optimized, when using a 15×15×15 Monkhorst-Pack k-point grid for Brillouin zone sampling, to be a=2.468 Å. The nitrogen doping models are two edged graphene models with p(5×6) periodicity in the X and Y directions and the edged C atoms are saturated by H atoms. Co-pyrrolic N_4 model is a graphene cluster in a box of 20Å×20Å×15Å nd doped with 4 pyrrolic N atoms and 1 Co atom. The CoNC model is built in reference to the previous report.[7] During structural optimizations, the gamma point in the Brillouin zone was used for k-point sampling, and all atoms were allowed to relax.

The adsorption energy (E_{ad}) of adsorbate A was defined as

$$E_{ad} = E_{A/surf} - E_{surf} - E_{A(g)}$$

where $E_{A/surf}$, E_{surf} and $E_{A(g)}$ are the energy of adsorbate A adsorbed on the surface, the energy of clean surface, and the energy of isolated A molecule in a cubic periodic box with a side length of 20 Å and a 1×1×1 Monkhorst-Pack k-point grid for Brillouin zone sampling, respectively.

Catalyst characterizations

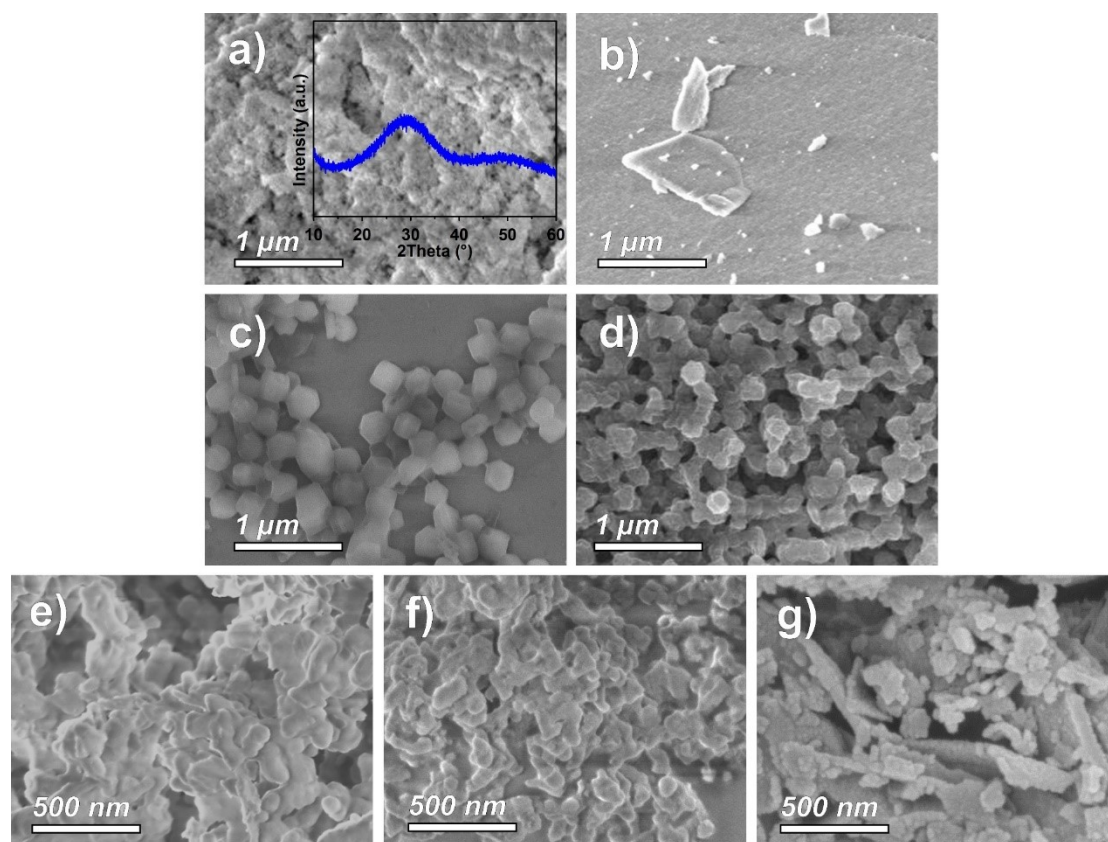**Fig. S1** SEM images of studied catalysts

Fig. S1 SEM images of studied catalysts. (a) ZrCP, insert: XRD pattern; (b) ZrNC; (c) ZIF-67; (d) CoNC; (e) Al-MCM-41; (f) ZrNC-MCM; (g) CoNC-MCM.

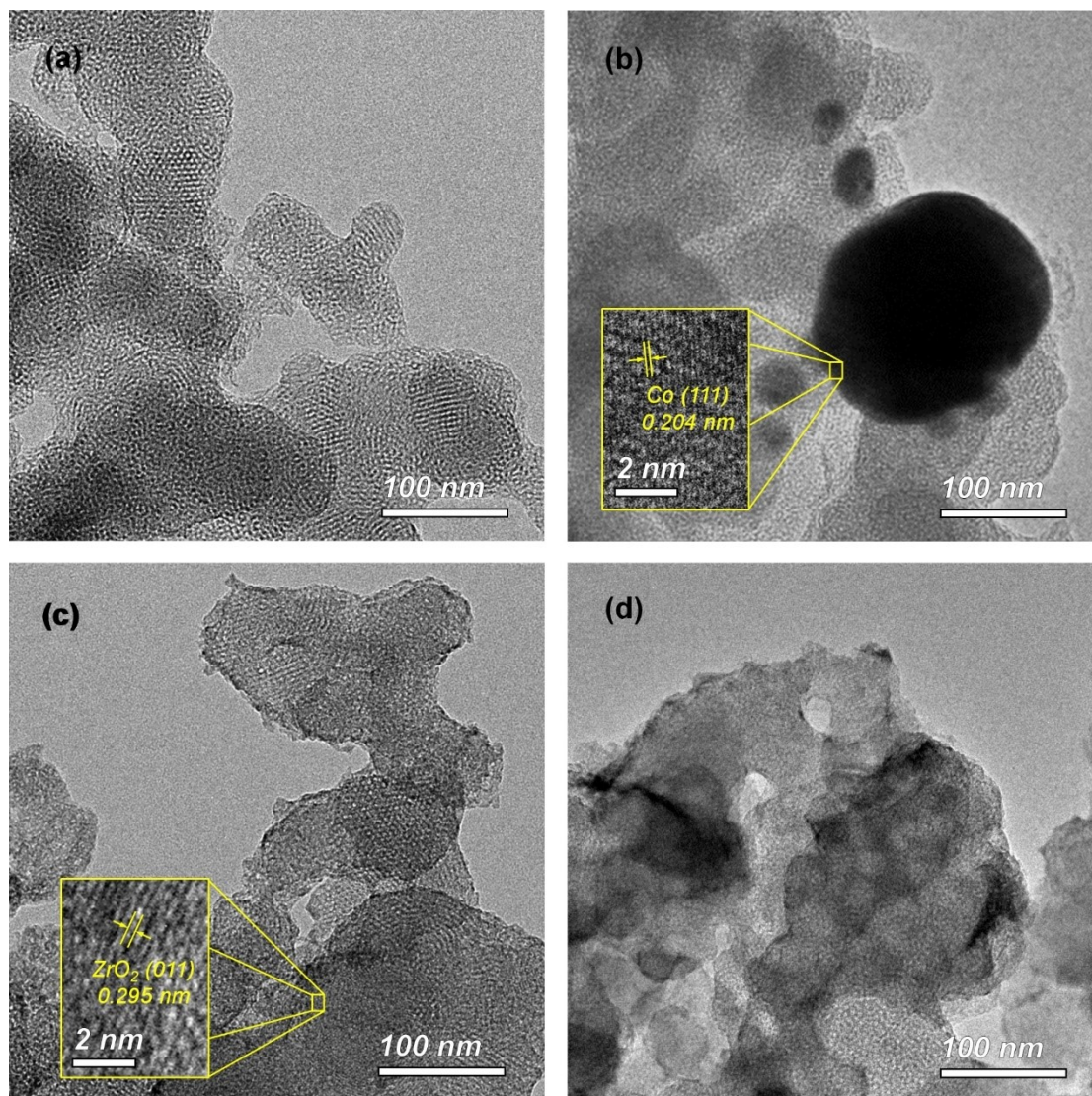**Fig. S2** TEM images of studied catalysts

Fig. S2 TEM images of studied catalysts. (a) Al-MCM-41; (b) CoNC-MCM; (c) ZrNC-MCM; (d) CoZrNC-MCM.

Fig. S3 N$_2$ adsorption/desorption isotherms
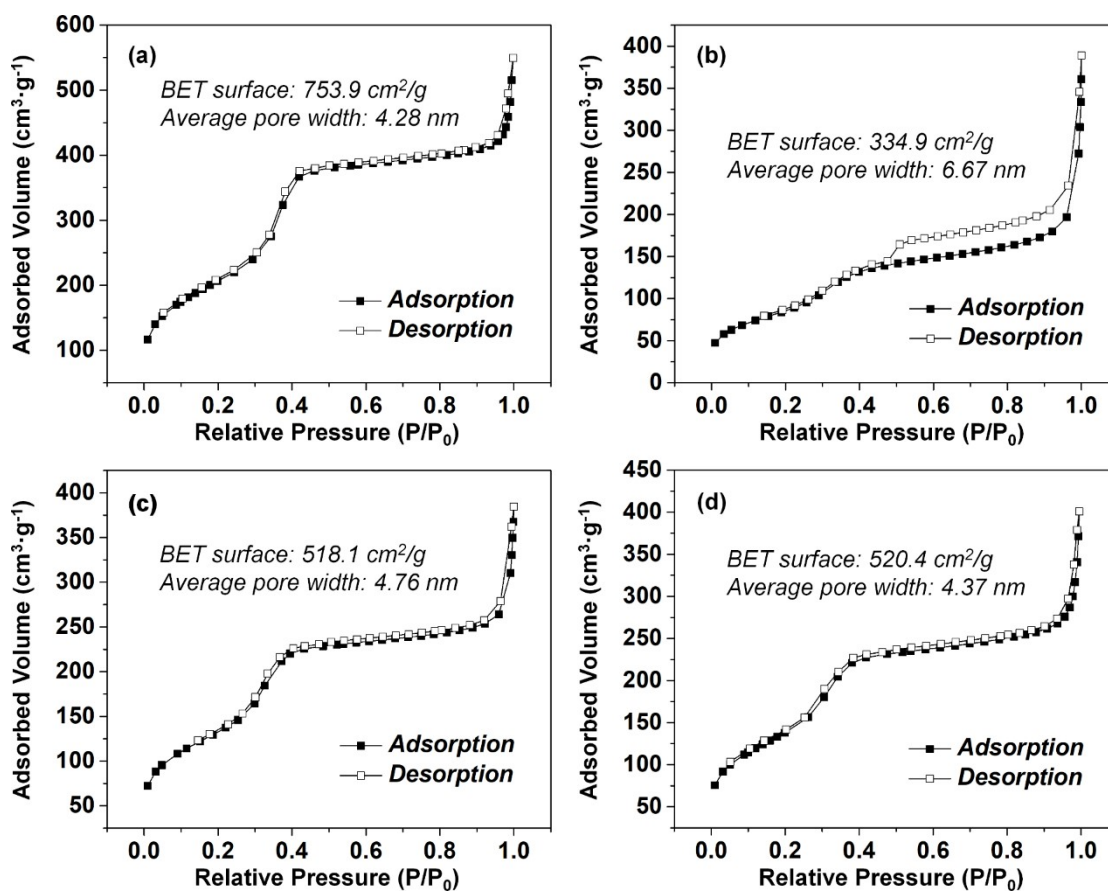
Fig. S3 N$_2$ adsorption/desorption isotherms. (a) Al-MCM-41; (b) CoNC-MCM; (c) ZrNC-MCM; (d) CoZrNC-MCM.

Fig. S4 XPS spectra of Co 2p3/2

Fig. S4 XPS spectra of Co 2p3/2. (a) CoNC; (b) CoNC-MCM; (c) CoZrNC-MCM.

Fig. S5 XPS spectra of Zr 3d

Fig. S5 XPS spectra of Zr 3d. (a) ZrNC; (b) ZrNC-MCM; (c) CoZrNC-MCM.

11

Fig. S6 XPS spectra of O 1s

Fig. S6 XPS spectra of O 1s. (a) Al-MCM-41; (b) CoNC-MCM; (c) ZrNC; (d) ZrNC-MCM; (e) CoZrNC-MCM.

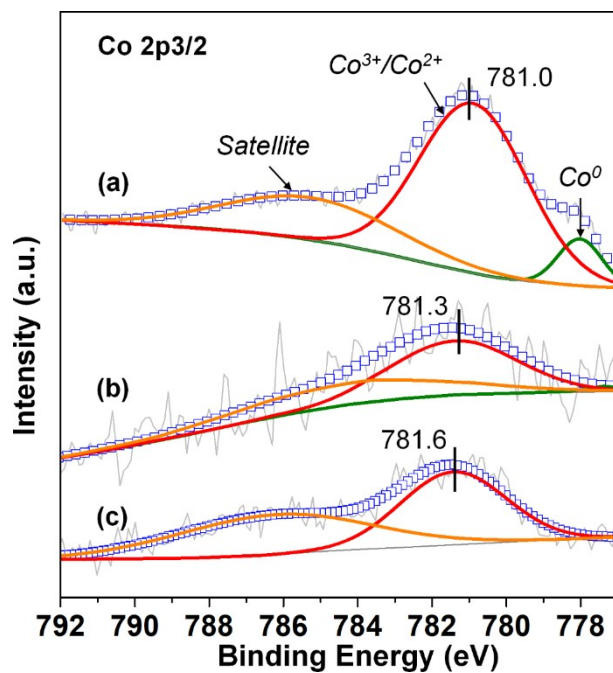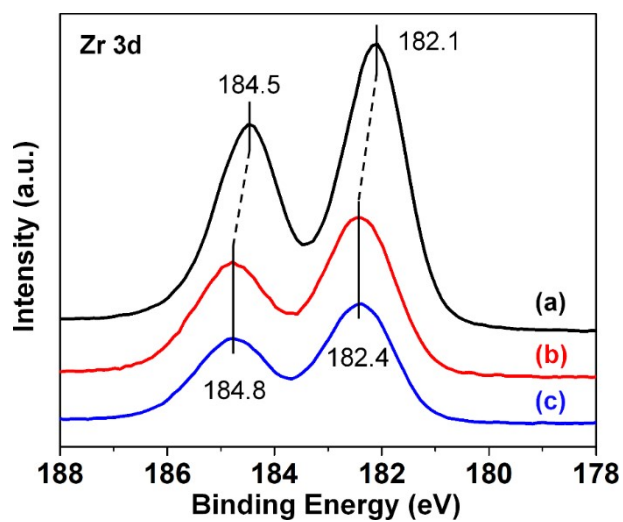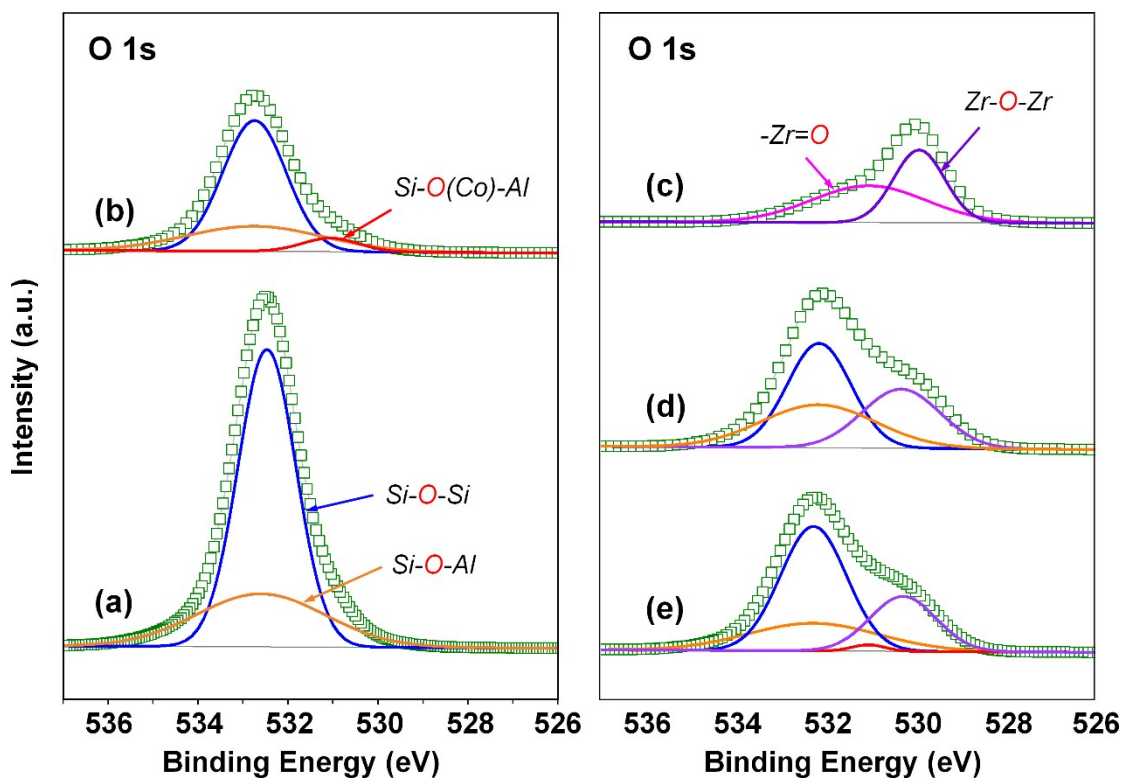**Fig. S7** Composition and distribution of acid sites over the studied catalyst

(a)

Acid type	Temperature, ºC	Conc., mmol/g
Weak	92, 110, 137, 206	0.36, 0.28, 0.39, 0.50
Moderate	402	0.59
Strong	558	0.17

(b)

Acid type	Temperature, ºC	Conc., mmol/g
Weak	93, 119	0.31, 0.39
Moderate	465	0.33
Strong	543, 619	0.37, 1.33

(c)

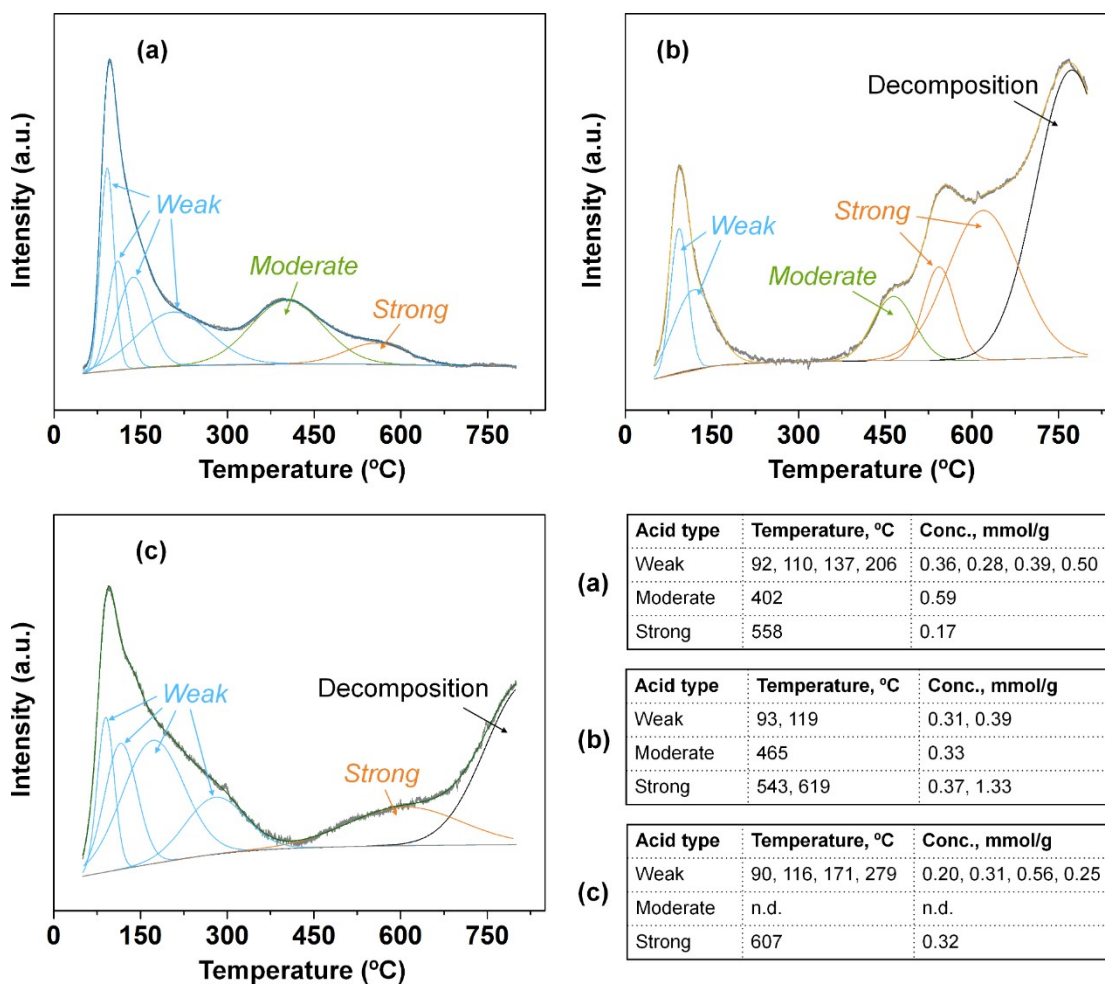| Acid type	Temperature, ºC	Conc., mmol/g
Weak	90, 116, 171, 279	0.20, 0.31, 0.56, 0.25
Moderate	n.d.	n.d.
Strong	607	0.32

Fig. S7 Composition and distribution of acid sites over the studied catalyst. (a) ZrNC-MCM; (b) CoNC-MCM; (c) CoZrNC-MCM.

Qualitative analysis of liquid products

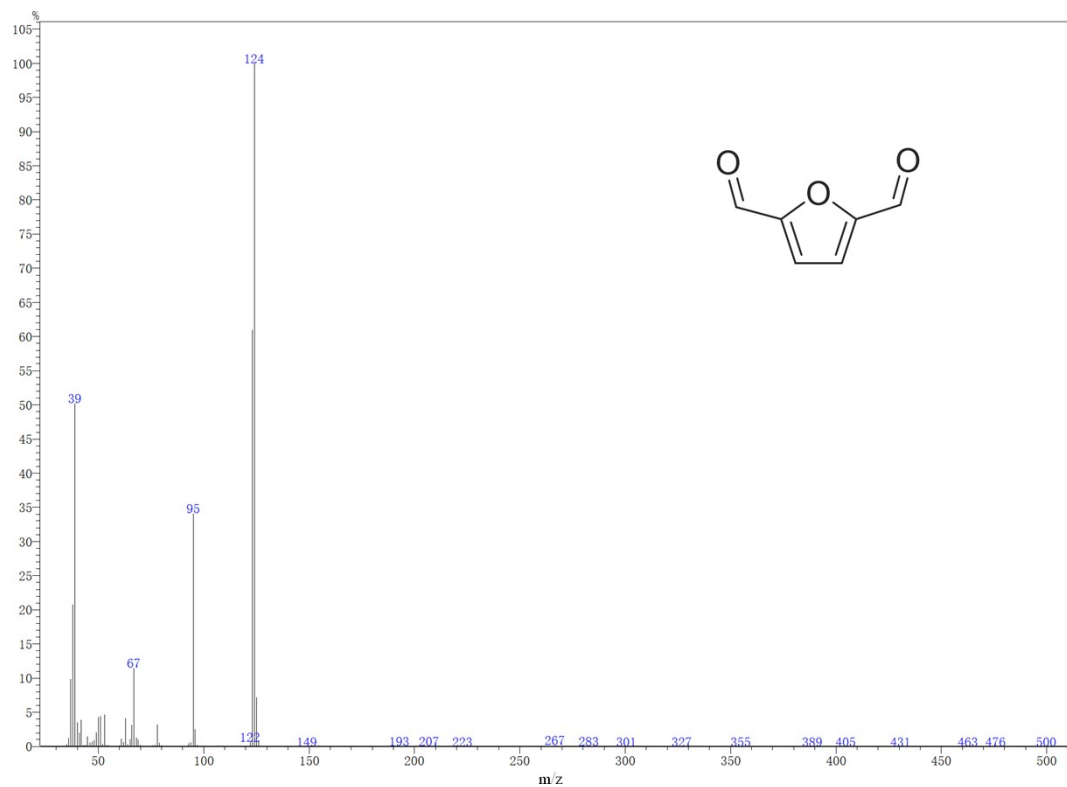**Figs. S8-S11** MS patterns of DFF, AFF, dimethyl sulfide and dimethyl disulfide
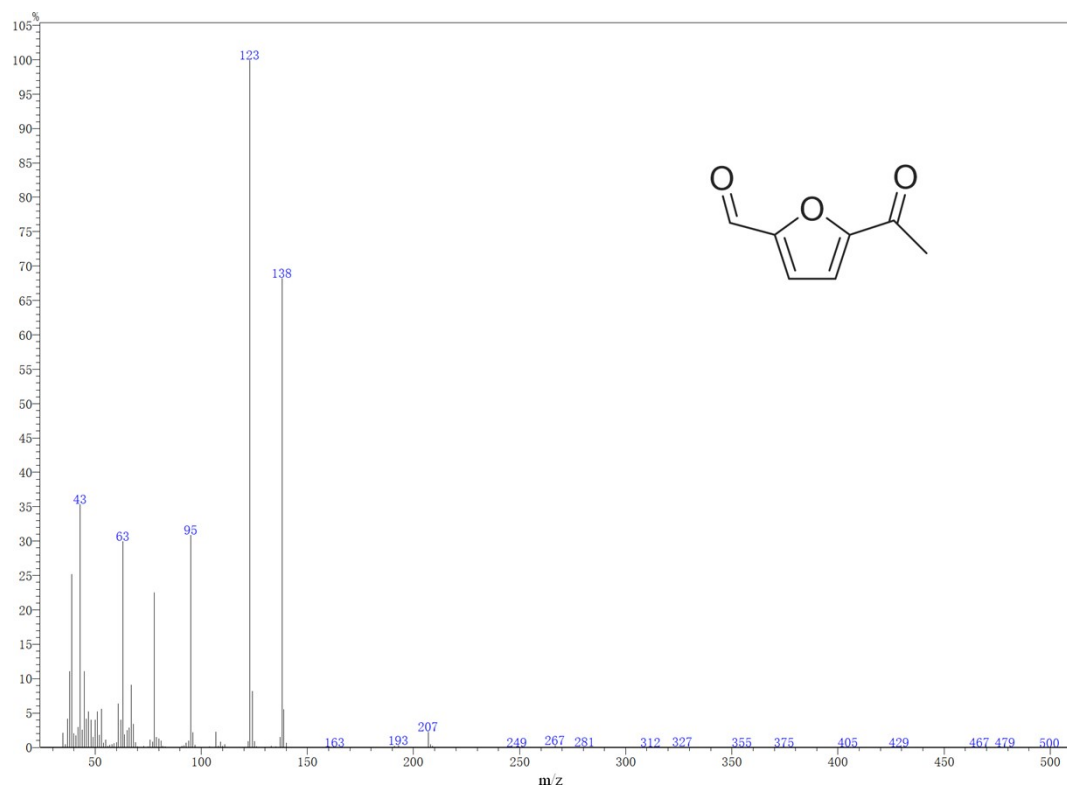

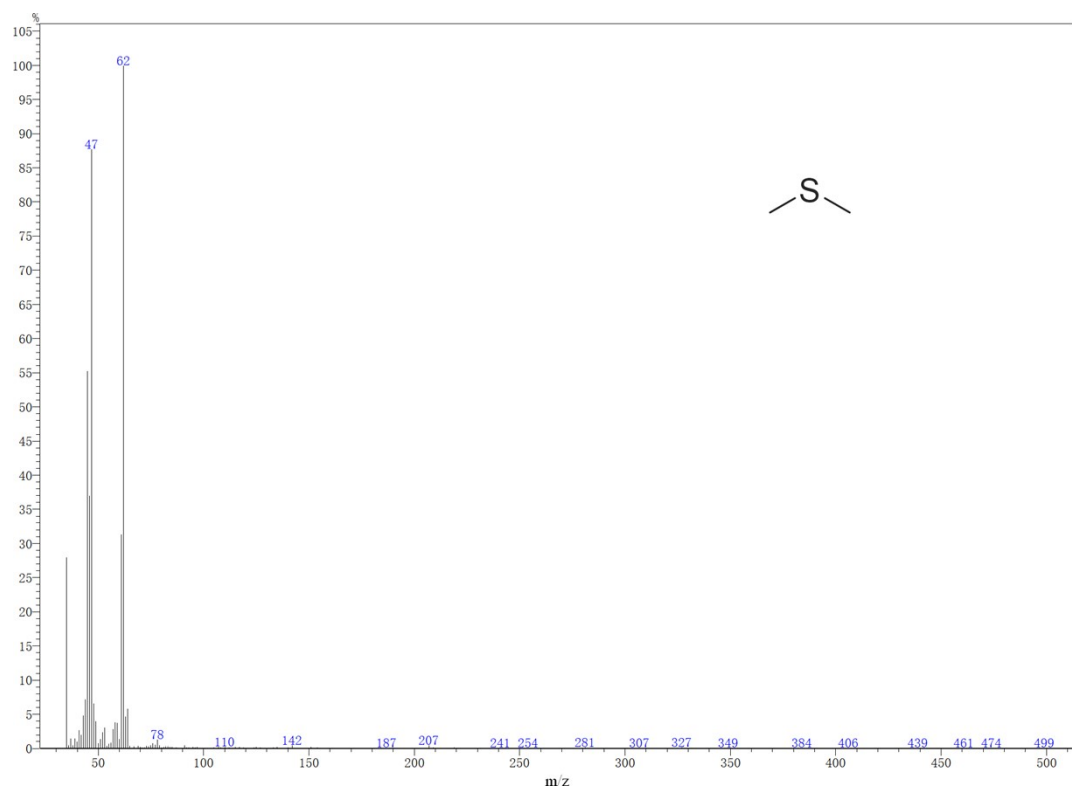**Fig. S8** MS pattern of DFF.

Fig. S9 MS pattern of AFF.

14

Fig. S10 MS pattern of dimethyl sulfide.
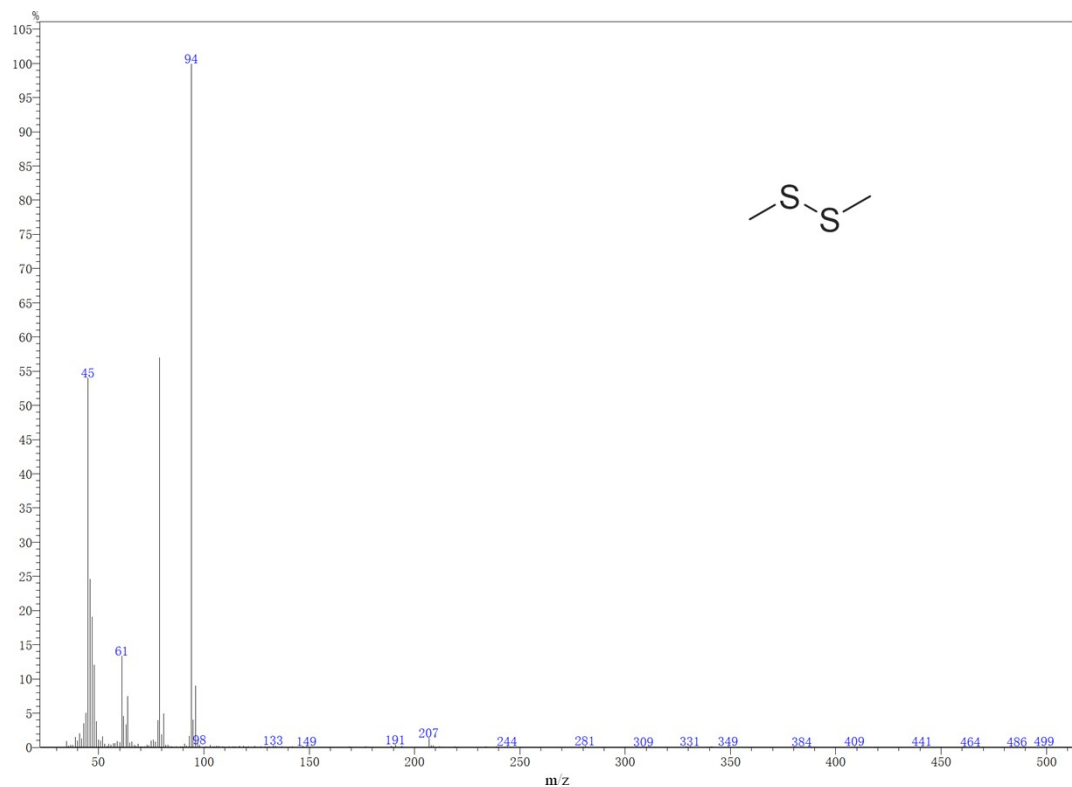
Fig. S11 MS pattern of dimethyl disulfide.

Adsorption energy calculation and reaction mechanisms

Fig. S12 Adsorption energy calculation of O_2 and DMSO

(a) E_{ad}= 3.74 eV   **(b)** E_{ad}= -0.05 eV

C ○   O ●
N ●   S ●   Co ●

(e) E_{ad}= -0.67 eV

(c) E_{ad}= 0.67 eV   **(d)** E_{ad}= 0.27 eV
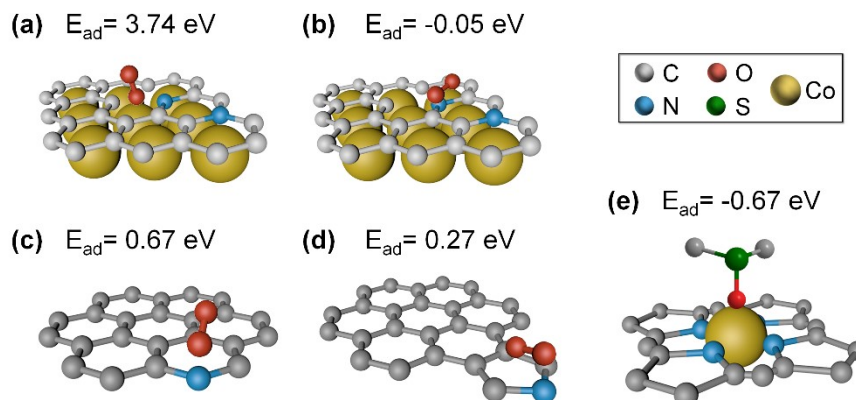
Fig. S12 Adsorption energy calculation of O_2 and DMSO. (a) O_2 adsorption on Co; (b) O_2 adsorption on NC; (c) O_2 adsorption on pyridinic N; (d) O_2 adsorption on pyrrolic N; (e) DMSO adsorption on Co of Co-pyrrolic N model.

Fig. S13 O_2 adsorption calculation based on Pyrrolic N model

(a) E_{ad}= -0.19 eV   **(b)** E_{ad}= -1.51 eV

Double-tooth adsorption   Single-tooth adsorption

Pyrrolic N ●
O ●   C ○

Fig. S13 O_2 adsorption calculation based on Pyrrolic N model. (a) O_2 double-tooth adsorption on N-C site; (b) O_2 single-tooth adsorption on N-C site.

Fig. S14 Plausible reaction mechanisms for HMF oxidation to DFF over CoZrNC-MCM
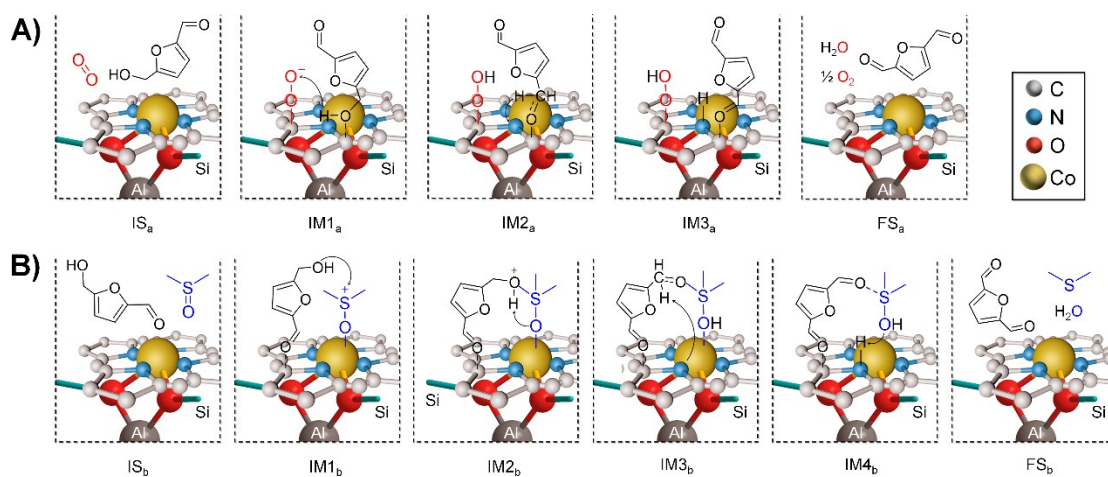
Fig. S14 Plausible reaction mechanisms for HMF oxidation to DFF over CoZrNC-MCM.

(a) O_2 as the sole oxidant; (b) DMSO as the sole oxidant.

Catalytic performance

Fig. S15 XRD patterns of fresh and spent catalysts.
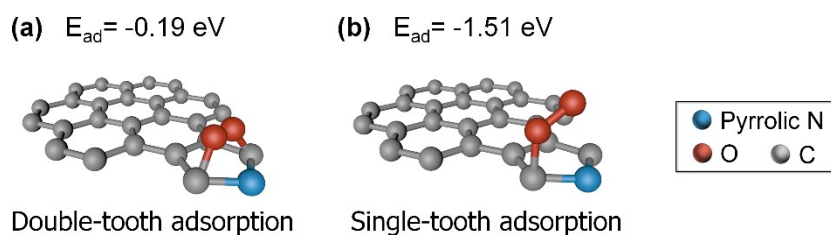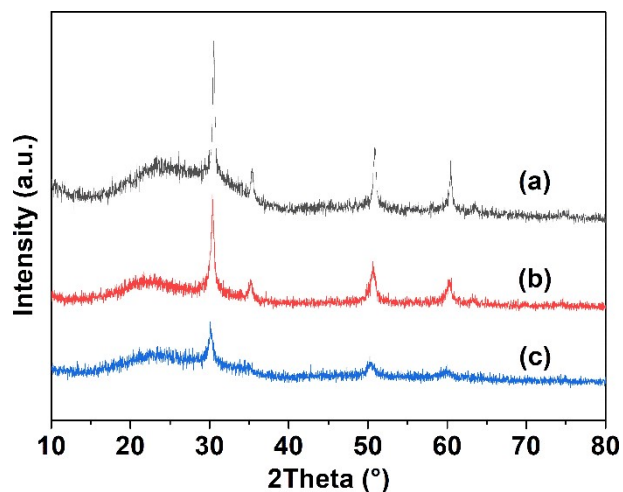

Fig. S15 XRD patterns of fresh and spent catalysts. (a) fresh CoZrNC-MCM, (b) spent CoZrNC-MCM after 2nd cycle; (c) spent CoZrNC-MCM after 5th cycle.

Fig. S16 Catalytic performance of CoZrNC-MCM for the direct conversion of fructose to DFF in the atmosphere.
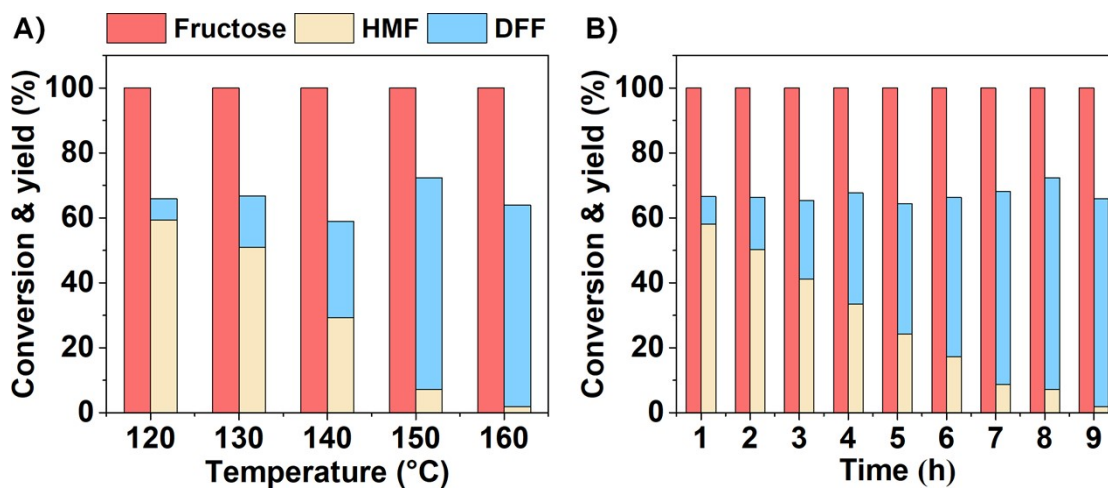
Fig. S16 Catalytic performance of CoZrNC-MCM for the direct conversion of fructose to DFF in the atmosphere. Effects of **A)** reaction temperature and **B)** time. Reaction condition: 0.2 g Fructose, 0.08 g CoZrNC-MCM, 19.8 g DMSO, 150 ºC and 8 h.

Control experiments

Scheme S1 Control experiments over CoZrNC-MCM catalyst

Scheme S1 Control experiments over CoZrNC-MCM catalyst.

Comparative studies

Table S1 Comparative studies for DFF synthesis from HMF over non-noble catalysts.

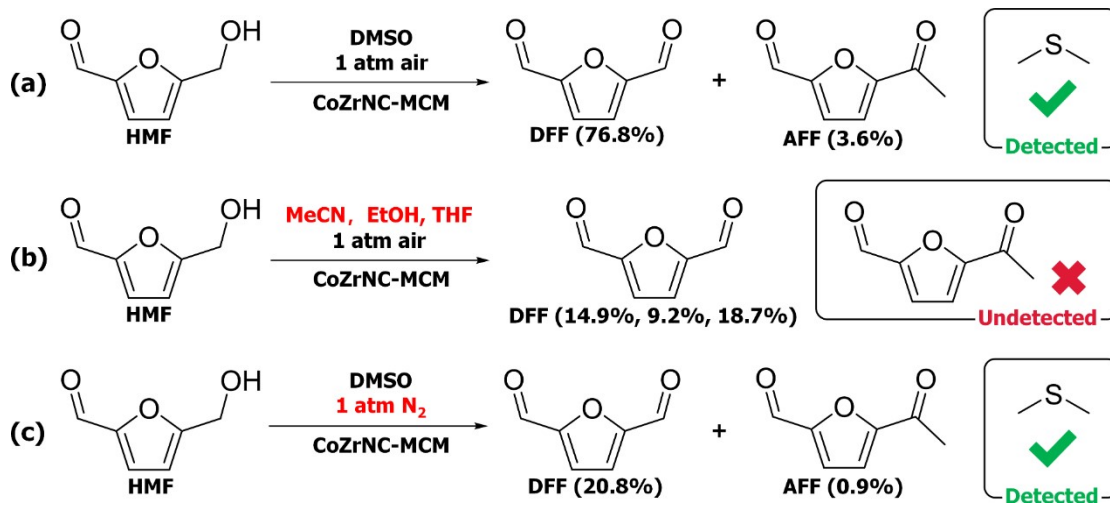| No.	Catalyst	Solvent	Oxidant and pressure, bar	T, ºC; t, h	DFF yield, %	Productivity, mmol·g^{-1}·h^{-1}	Ref.
1	Y-VOPO$_4$	DMSO	Air, 1	150; 19	41	0.4	[8]
2	V$_2$O$_5$	DMSO	Air, 1	150; 13	43	0.7	[8]
3	VO(H$_2$PO$_4$)	DMSO	Air, 1	120; 10	84	0.8	[9]
4	N-doped AC 8	Ethanol	Air, 1	80, 15	22	0.1	[10]
5	N-MnO$_2$	Toluene	O$_2$, 1	25; 6	100	0.6	[11]
6	S-PANI-FeVO$_4$	DMSO	O$_2$, 1	140; 24	>99	0.3	[12]
7	Mn$_6$Fe$_1$O$_x$	DMF	O$_2$, 15	110; 5	95	2.4	[13]
8	Mn$_{0.5}$-Co$_3$O$_4$	Toluene	O$_2$, 1	60; 6	97	0.4	[14]
9	Cs/MnO$_x$	DMF	O$_2$, 10	100; 12	95	1.9	[15]
10	Mn$_{0.7}$Cu$_{0.05}$Al$_{0.25}$	H$_2$O	O$_2$, 8	90; 24	78	0.7	[16]
11	MgO·CeO$_2$	H$_2$O	O$_2$, 9	110; 15	96	1.3	[17]
12	Cs$_2$H$_2$PMo$_{11}$VO$_{40}$	DMSO	O$_2$, 1	120; 6	99	1.1	[18]
13	CeCu(OH)$_6$Mo$_6$O$_{18}$	p-chlorotoluene	O$_2$, 1	130; 8	99	0.4	[19]
14	HPMoV/SiO$_2$	DMSO	O$_2$, 10	120; 8	89	1.4	[20]
15	SBA-Py-VO-2	Triflurotoluene	O$_2$, 1	130; 24	30	0.5	[21]
16	Polyaniline-VO(acac)2	4-chlorotoluene	O$_2$, 1	110; 12	86	0.7	[22]
17	SBA-NH$_2$-VO^{2+}+SBA-NH$_2$-Cu^{2+}	4-chlorotoluene	O$_2$, 1	110; 12	63	0.3	[23]
18	HPMoV@surf (4)/CeO$_2$	DMSO	O$_2$, 10	120; 6	95	1.9	[24]
19	HPMoV/CS-f	DMSO	O$_2$, 8	120; 6	94	2.1	[25]
20	FeN$_x$/C-900	DMF	O$_2$, 5	80; 10	97	0.2	[26]
21	Co$_{0.05}$/N-C-800	Toluene	O$_2$, 1	100; 30	94	0.5	[27]
22	VO$_2$-PANI/CNT	DMSO	O$_2$, 10	120; 11	96	0.9	[28]
23	P-C-N-5-800	Acetonitrile	O$_2$, 10	120; 9	100	1.1	[29]
24	Mn(III)-salen-5	CH$_2$Cl$_2$	NaOCl	25; 24	89	0.001	[30]
25	Fe salen/SBA-15	H$_2$O	H$_2$O$_2$	25; 1.7	2	0.06	[31]
26	NaI	DMSO	DMSO	150; 18	7	0.09	[32]
27	NaCl	DMSO	DMSO	150; 18	10	0.3	[32]
28	NaBr	DMSO	DMSO	150; 18	85	1.5	[32]
29	Co$_2$Zr$_1$NC-MCM	DMSO	DMSO, air	140; 9	85.1	1.9	This work

Table S2 Comparative studies for DFF synthesis from fructose using DMSO as oxygen source.

Catalyst	Additive	T, ºC	t, h	DFF yield, %	Productivity, mmol·g^{-1}·h^{-1}	Carbon balance, %	Ref.
-	NaBr	150	23	67	0.85	67	[32]
TFP-DABA	KBr	100	12	65	1.00	65	[33]
Amberlite 120 H	KBr	120	12	80	0.63	80	[34]
CoZrNC-MCM	-	150	8	65.2	1.13	75.4	This work

Supplementary references

1. G. Kresse and J. Furthmuller, *Comp. Mater. Sci.*, 1996, **6**, 15-50.
2. G. Kresse and J. Furthmüller, *Phys. Rev. B*, 1996, **54**, 11169-11186.
3. J. P. Perdew and K. Burke, *Phys. Rev. Lett.*, 1996, **77**, 3865-3868.
4. G. Kresse and D. Joubert, *Phys. Rev. B*, 1999, **59**, 1758-1775.
5. P. E. Blöchl, *Phys. Rev. B*, 1994, **50**, 17953-17979.
6. S. Grimme, J. Antony, S. Ehrlich and H. Krieg, *J. Chem. Phys.*, 2010, **132**, 154104.
7. Y. Feng, W. Jia, G. Yan, X. Zeng, J. Sperry, B. Xu, Y. Sun, X. Tang, T. Lei and L. Lin, *J. Catal.*, 2020, **381**, 570-578.
8. G. A. Halliday, R. J. Young and V. V. Grushin, *Org. lett.*, 2003, **5**, 2003-2005.
9. J. Lai, K. Liu, S. Zhou, D. Zhang, X. Liu, Q. Xu and D. Yin, *RSC Adv.*, 2019, **9**, 14242-14246.
10. H. Watanabe, S. Asano, S. I. Fujita, H. Yoshida and M. Arai, *ACS Catal.*, 2015, **5**, 2886-2894.
11. Q. Ke, Y. Jin, F. Ruan, M. N. Ha, D. Li, P. Cui, Y. Cao, H. Wang, T. Wang and V. N. Nguyen, *Green Chem.*, 2019, **21**, 4313-4318.
12. A. Kumar and R. Srivastava, *Mol. Catal.*, 2019, **465**, 68-79.
13. H. Liu, X. Cao, J. Wei, W. Jia, M. Li, X. Tang, X. Zeng, Y. Sun, T. Lei and S. Liu, *ACS Sustain. Chem. Eng.*, 2019, **7**, 7812-7822.
14. Q. Ke, D. Yi, Y. Jin, F. Lu and X. Wang, *ACS Sustain. Chem. Eng.*, 2020, **8**, 5734-5741.
15. Z. Yuan, B. Liu, P. Zhou, Z. Zhang and Q. Chi, *Catal. Sci. Technol.*, 2018, **8**, 4430-4439.
16. F. Neatu, N. Petrea, R. Petre, V. Somoghi, M. Florea and V. I. Parvulescu, *Catal. Today*, 2016, **278**, 66-73.
17. M. Ventura, F. Lobefaro, E. Giglio, M. Distaso, F. Nocito and A. Dibenedetto, *ChemSusChem*, 2018, **11**, 1305-1315.
18. R. Liu, J. Chen, L. Chen, Y. Guo and J. Zhong, *ChemPlusChem*, 2014, **79**, 1448-1454.
19. J. Xu, T. Su, Z. Zhu, N. Chen, D. Hao, M. Wang, Y. Zhao, W. Ren and H. Lu, *Chem. Eng. J.*, 2020, **396**, 125303.
20. J. Zhao, J. Anjali, Y. Yan and J. Lee, *ChemCatChem*, 2017, **9**, 1187-1191.
21. O. C. Navarro, A. C. Canós and S. I. Chornet, *Top. Catal.*, 2009, **52**, 304-314.
22. F. Xu and Z. Zhang, *ChemCatChem*, 2015, **7**, 1470-1477.
23. X. Liu, J. Xiao, H. Ding, W. Zhong, Q. Xu, S. Su and D. Yin, *Chem. Eng. J.*, 2016, **283**, 1315-1321.
24. Y. Li, YimingLi, PeiliCao, PingWang, XiaohongGuan, Hongyu, *Appl. Catal., A*, 2019, **583**, 117122.
25. Y. Li, P. Li, P. Cao, Y. Li, X. Wang and S. Wang, *ChemSusChem*, 2019, **12**, 3515-3523.

26. J. Zhang, S. Nagamatsu, J. Du, C. Tong, H. Fang, D. Deng, X. Liu, K. Asakura and Y. Yuan, *J. Catal.*, 2018, **367**, 16-26.

27. X. Zhao, Y. Zhou, K. Huang, C. Li and D. J. Tao, *ACS Sustain. Chem. Eng.*, 2019, **7**, 1901-1908.

28. Y. Guo and J. Chen, *ChemPlusChem*, 2015, **80**, 1760-1768.

29. H. Zhang, J. H. Clark, T. Geng, H. Zhang and F. Cao, *ChemSusChem*, 2021, **14**, 456-466.

30. A. S. Amarasekara, D. Green and E. Mcmillan, *Catal. Commun.*, 2008, **9**, 286-288.

31. D. Martinez-Vargas, J. De La Rosa, L. Sandoval-Rangel, J. Luis Guzman-Mar, M. A. Garza-Navarro, C. J. Lucio-Ortiz and D. A. De Haro-Del Rio, *Appl. Catal., A*, 2017, **547**, 132-145.

32. C. Laugel, B. Estrine, J. Le Bras, N. Hoffmann, S. Marinkovic and J. Muzart, *ChemCatChem*, 2014, **6**, 1195-1198.

33. Y. Peng, Z. Hu, Y. Gao, D. Yuan, Z. Kang, Y. Qian, N. Yan and D. Zhao, *ChemSusChem*, 2015, **8**, 3208-3212.

34. A. S. Chauhan, A. Kumar, R. Bains and P. Das, *Green Chem.*, 2022, **24**, 6125-6130.